Bioactive Materials 24 (2023) 69–80

Contents lists available at ScienceDirect

Bioactive Materials

journal homepage: www.keaipublishing.com/en/journals/bioactive-materials

# Construction of multifunctional hydrogel with metal-polyphenol capsules for infected full-thickness skin wound healing

Nanbo Liu [a,f,1], Shuoji Zhu [a,c,f,1], Yuzhi Deng [a,d,f,1], Ming Xie [a,f,1], Mingyi Zhao [a,f], Tucheng Sun [a,f], Changjiang Yu [a,f], Ying Zhong [d], Rui Guo [e,**], Keluo Cheng [d,***], Dehua Chang [b,****], Ping Zhu [a,d,f,*]

[a] Guangdong Cardiovascular Institute, Guangdong Provincial People's Hospital, Guangdong Academy of Medical Sciences, Guangzhou, Guangdong, 510100, China
[b] University of Tokyo Hospital Department of Cell Therapy in Regenerative Medicine, Tokyo, 113-8666, Japan
[c] University of Tokyo, Tokyo, 113-8666, Japan
[d] Affiliated Hospital of Guangdong Medical University, Zhanjiang, Guangdong, 524001, China
[e] Key Laboratory of Biomaterials of Guangdong Higher Education Institutes, Guangdong Provincial Engineering and Technological Research Centre for Drug Carrier Development, Department of Biomedical Engineering, Jinan University, Guangzhou, 510632, China
[f] Guangdong Provincial Key Laboratory of Pathogenesis, Targeted Prevention and Treatment of Heart Disease, Guangzhou Key Laboratory of Pathogenesis, Targeted Prevention and Treatment of Heart Disease, Guangzhou, Guangdong, 510100, China

ARTICLE INFO

*Keywords:*
Metal polyphenol network
Copper
Epigallocatechin-3-gallate
Infected wound healing

ABSTRACT

Damaged skin cannot prevent harmful bacteria from invading tissues, causing infected wounds or even severe tissue damage. In this study, we developed a controlled-release antibacterial composite hydrogel system that can promote wound angiogenesis and inhibit inflammation by sustained releasing Cu-Epigallocatechin-3-gallate (Cu-EGCG) nano-capsules. The prepared SilMA/HAMA/Cu-EGCG hydrogel showed an obvious inhibitory effect on *Escherichia coli (E. coli)* and *Staphylococcus aureus (S. aureus)*. It could also promote the proliferation and migration of L929 fibroblasts. *In vivo* full-thickness infected wound healing experiments confirmed the angiogenesis and inflammation regulating effect. Accelerate collagen deposition and wound healing speed were also observed in the SilMA/HAMA/Cu-EGCG hydrogel treated group. The findings of this study show the great potential of this controlled-release antibacterial composite hydrogel in the application of chronic wound healing.

## 1. Introduction

The skin is the largest multilayered organ of the human body, including the epidermis and dermis, as well as a barrier to protect the body from excessive evaporation of water and pathogens [1–3]. However, once the entire epidermis are seriously injured, the skin will lose its most basic protection, and may be accompanied by severe microbial infection, lading to prolonged healing process or form nonfunctional scars [4–7]. Antibiotics have been widely used to treat this problem, but it inevitably leads to the emergence of drug resistance [8,9]. Ideal wound dressings need to provide a solid barrier against external infections and guide skin cell integration and infiltration for wound healing [10,11]. Adequate mechanical strength and moisture retention ability, good biocompatibility and easy adhesive for cells are all essential for wound dressing [12,13]. Among these various dressings, polymeric hydrogels can maintain good hydrophilicity and have adjustable physical and biocompatibility, which are considered the most promising wound dressing candidate [14,15].

Hyaluronic acid (HA) is a natural polymer found in the human body that has good biocompatibility [16]. In the epidermal repair phase,

Peer review under responsibility of KeAi Communications Co., Ltd.
* Corresponding author. Guangdong Cardiovascular Institute, Guangdong Provincial People's Hospital, Guangdong Academy of Medical Sciences, Guangzhou, Guangdong, 510100, China.
** Corresponding author.
*** Corresponding author.
**** Corresponding author.
*E-mail addresses:* guorui@jnu.edu.cn (R. Guo), lml811@163.com (K. Cheng), dehua_chang@yahoo.com (D. Chang), tanganqier@163.com (P. Zhu).
[1] These authors contributed equally to this work.

https://doi.org/10.1016/j.bioactmat.2022.12.009
Received 30 November 2022; Received in revised form 9 December 2022; Accepted 9 December 2022

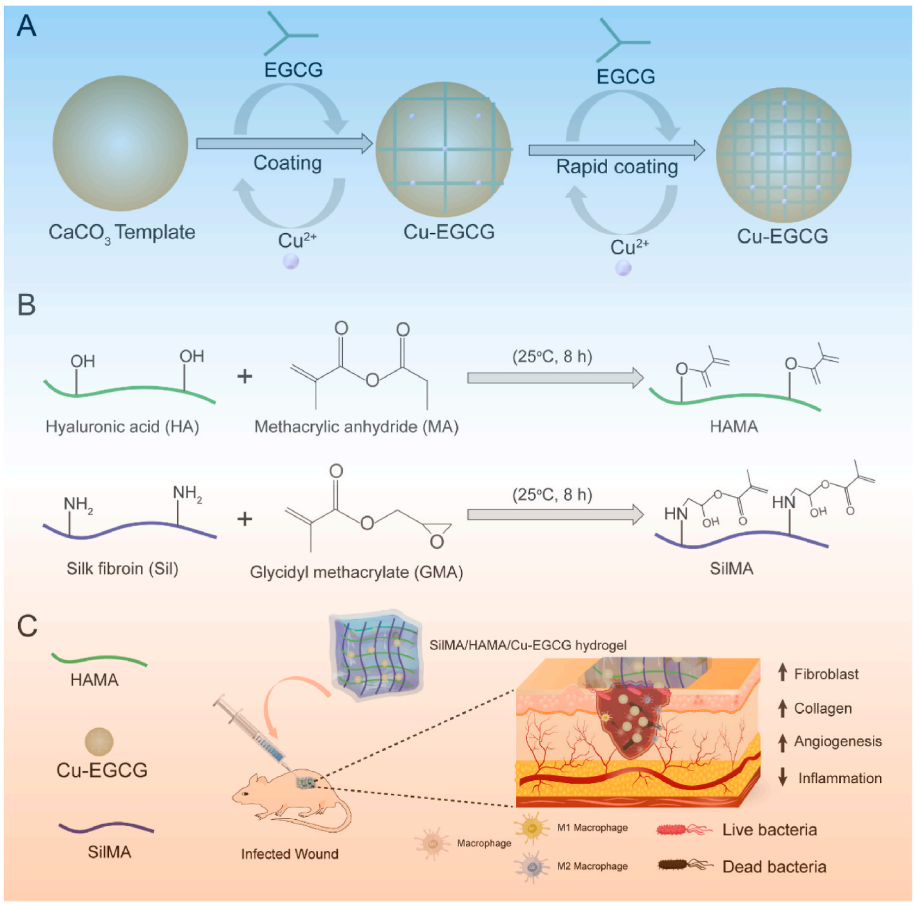


**Scheme 1.** (A) Schematic of the synthesis of Cu-EGCG. (B) Schematic illustration showing the synthesis of HAMA and SilMA. (C) Application of the SilMA/HAMA/Cu-EGCG hydrogel for infected wound healing and skin reconstruction.

CD44 receptors interact with HA, promoting the progression of a series of re-epithelialization processes, such as angiogenesis, cell migration, proliferation, deposition of type II collagen, adhesion to ECM components, and the recruitment of neutrophils [17,18]. However, their poor mechanical strength and low adhesion to cells hinder their application in the biomedical field [19]. Changing the molecular weight or developing HA-chemical derivatives are helpful to composite more adaptive hydrogels.

Silk fibroin (Sil), the fiber portion isolated from silkworms, has been explored for wound healing, bioartificial skin grafts and other biomedical applications due to its mechanical properties and excellent biocompatibility [20,21]. It is constituted by amino acid sequence Gly-Ser-Gly-Ala-Gly-Ala [22], thus has high affiliation to cells and tissue. The β-sheet structure of Sil can be modified by physical or chemical cross-linking methods, such as methacryloyl substitution [23]. Therefore, we plan to form a hydrogel with a double network structure using methacrylated hyaluronic acid (HAMA) cross-linking with methacrylate-modified silk fibroin (Sil-MA) to prepare a composite hydrogel with good biocompatibility and mechanical properties that better meets the application requirements of wound dressings.

Epigallocatechin 3-gallate (EGCG) is the most abundant catechin in tea [24]. Researchers have found that EGCG exhibits a wide range of beneficial effects, including anti-inflammatory, antiaging, antioxidative, angiogenesis, anticarcinogenic, and antimicrobial effects [25,26]. However, shortcomings such as low bioavailability and excessive metabolism of EGCG limit its development [27]. A wide variety of metal ions and phenolic molecules yielding modular libraries of metal−phenolic complexes are emerging as a strategy for assembling drug delivery platforms [28]. Among many metal ions, we chose copper ions as the metal ligands of the complex. The robust chelation of copper ions with EGCG not only imparted antibacterial and anti-inflammatory abilities but also promoted wound angiogenesis, which is more conducive to accelerating wound healing [25].

Here, we aim to construct a metal polyphenol capsule (Cu-EGCG), which was formed by a simple one-step ion/molecular assembly process and loaded into a SilMA/HAMA hydrogel wound dressing to achieve continuous release of EGCG and copper ions (Scheme 1). The stability, swelling, compressibility and rheological properties of hydrogels were systematically studied and evaluated. The *in vitro* cytotoxicity of SilMA/HAMA/Cu-EGCG hydrogel to L929 fibroblast cells was also evaluated. In addition, the antibacterial activity against *Escherichia coli (E. coli)* and *Staphylococcus aureus (S. aureus)* was also further tested. Finally, the therapeutic effect of the HAMA/SilMA/CuEGCG hydrogel on the skin defect model was evaluated by wound repair, histopathological examination, and immunofluorescence staining. Few hydrogels were reported to contain inherent properties that promote angiogenesis while preventing bacterial infection, this unique multifunctional hydrogel will show effective anti-infective ability, enhance angiogenic activity, and accelerated infected skin wounds healing speed through immunoregulation.

## 2. Materials and methods

### 2.1. Materials

Cocoons were obtained from Xiaoya Wei Silkworm Business Department (Guangxi, China). Sodium carbonate (AR, 99%) was purchased from Aladdin (Shanghai, China). Lithium bromide, methacrylic

anhydride (MA), glycidyl methacrylate (GMA) and 4-dimethylaminopyridine were obtained from Macklin Inc. (Shanghai, China). Hyaluronic acid (200 kDa) was purchased from Freda Biochem Co., Ltd. (Shandong, China). *Escherichia coli* (*E. coli* ATCC 8099) and *Staphylococcus aureus* (*S. aureus* ATCC 6538) were purchased from Luwei Microbial Sci&Tech Co., Ltd. (Shanghai, China). LB agar medium was obtained from Guangdong Huankai Microbial Science and Technology Co., Ltd. (Guangzhou, China). Dulbecco's modified Eagle's medium (DMEM) and fetal bovine serum (FBS) were purchased from Gibco (USA).

### 2.2. Synthesis of Cu-EGCG

First, PSS was dissolved in 20 mM $CaCl_2$ and $Na_2CO_3$ solution at a concentration of 1 mg/mL. Then, $Na_2CO_3$ solution was quickly added to CaCl2 solution (the ratio of the volume is v: v = 1: 1), stirred violently, centrifuged for 5 min to collect the sediment, and washed with deionized water 3 times. An additional 500 μL EGCG (0.5 mL, 24 mM), $CuCl_2$ (0.5 mL, 24 mM) aqueous solution, and 5 mL MOPS buffer (100 mM, pH 8.0) were added to each sample and vortexed again for 30 s. Excessive EGCG and $CuCl_2$ were removed by washing to obtain $CaCO_3$ particles coated with Cu-EGCG. The above steps were repeated 2 times to obtain $CaCO_3$ particle-coated Cu-EGCG with three layers.

### 2.3. Synthesis of SilMA and HAMA

Silk fibroin was obtained after optimization as previously described [29]. 10 g of cocoons was immersed in 1 L of 0.05 M $Na_2CO_3$ solution, boiled for 30 min, and then washed with distilled water several times to obtain degummed silk fibroin. Then, the degummed silk fibroin (Sil) was dried in a drying box for 36 h. To obtain methacrylated silk fibroin (SilMA), 10 g degummed SF was dissolved in 9.3 M lithium bromide (LiBr) solution at 60 °C for 1 h and then slowly dripped with 6 mL glycidyl methacrylate (GMA). After 8 h of reaction, the solution was filtered through a magic filter cloth and dialyzed with distilled water in a dialysis bag (12000–14000 Da) for 3–5 days. The obtained solution was freeze-dried to obtain spongy SilMA.

Methacrylated hyaluronic acid (HAMA) was synthesized according to modified synthetic methods reported in the literature [30]. 1 g of HA was completely dissolved in 100 mL of ultra-pure water. Next, 3 mL of methacrylic anhydride (MA) was slowly dripped, and the pH was kept at approximately 8.5 by adding 5 mol/L sodium hydroxide. After 8 h of reaction at room temperature, the solution was dialyzed with distilled water in a dialysis bag (12000–14000 Da) for 3–5 days. The obtained solution was freeze-dried to obtain spongy HAMA.

### 2.4. Preparation of SilMA/HAMA hydrogels

First, a SilMA aqueous solution with a concentration of 10% was prepared, and HAMA solutions of different concentrations (1% (w/v), 1.5% (w/v), 2% (w/v)) were mixed in the SilMA solution at a volume ratio of 1:1. Next, a concentration of 0.1% LAP was added to the mixed solution as a photo initiator. The solution was irradiated with blue light (405 nm) for 10 s to induce photo crosslinking.

### 2.5. Characterization

#### 2.5.1. 1H NMR and SEM test

The nanoparticle size of Cu-EGCG was analyzed through DLS on a Zetasizer Nano-ZS (Malvern Instruments, Malvern, UK). The chemical structures of Sil, SilMA, HA, and HAMA were obtained by 1H NMR (600 MHz Inova-600, Varian, CA) utilizing D2O as the solvent. Fourier transform infrared spectroscopy (FTIR) spectra of Sil, SilMA, HA, and HAMA were recorded with FTIR spectroscopy (iS10, Thermo Electron, USA). The microscopic morphology of Cu-EGCG and freeze-dried hydrogels was observed by scanning electron microscopy (SEM; S-3400, Hitachi, Japan).

#### 2.5.2. Rheological and compression test

The rheological properties of the SilMA/HAMA hydrogel were determined using a rheometer instrument (Malvern, Worcestershire, UK). Rheological measurements were performed with a stainless-steel parallel plate rotor with a diameter of 25 mm. G′ characterizes the elastic modulus of the sample, and G″ characterizes the viscous modulus of the sample. Dynamic strain sweeps were performed from 0.1 to 10 rad/s at room temperature to determine the linear viscoelasticity range of the hydrogel, and the storage modulus (G′) and loss modulus (G″) curve were recorded.

#### 2.5.3. Mechanical properties analysis

For the compression tests, the cylindrical hydrogel samples (Φ12 mm × 6 mm) were placed between the self-levelling plates and compressed at a rate of 10 mm/min until the compression ratio was 80%.

#### 2.5.4. Swelling test

The swelling properties of hydrogels were evaluated by the gravimetric method. The SilMA/HAMA hydrogel was weighed ($W_0$) and then immersed in PBS solution at room temperature. After a fixed time, the swollen hydrogel was removed from water, dried with clean filter paper, and weighed ($W_t$). The swelling ratio was calculated using the following equation:

$$\text{Swelling ratio } (\%) = (W_t - W_0) / W_0 \times 100$$

#### 2.5.5. In vitro degradation test

The biodegradability of the hydrogel was studied by enzyme degradation experiments. Briefly, the hydrogels were immersed in PBS solution (pH = 7.4) containing 0 or 1000 U/mL lysozyme, and degradation was observed at 37 °C. At predetermined time intervals, the hydrogels were removed, washed with ultrapure water, lyophilized, and weighed ($W_t$). The weight remaining ratio of the hydrogel was calculated using the following equation:

$$\text{Weight remaining ratio } (\%) = W_t / W_0 \times 100$$

#### 2.5.6. In vitro $Cu^{2+}$ release

The release of $Cu^{2+}$ was detected by ICP–MS. Briefly, 1 mL of hydrogel was placed in 10 mL of PBS solution (pH = 7.4) at 37 °C, the release medium was collected at different times, and the same volume of PBS was replenished. The content of $Cu^{2+}$ in the collected PBS supernatant was detected by ICP–MS, and the cumulative release rate was calculated using the following equation:

$$\text{Cumulative release ratio } (\%) = \text{Cumulative released amount } / \text{Total loaded mass} \times 100$$

### 2.6. In vitro antimicrobial activity assay

Gram-positive bacteria (*Staphylococcus aureus*, *S. aureus*) and gram-negative bacteria (*Escherichia coli*, *E. coli*) were selected as model bacteria for the experiment. First, the hydrogel sample (200 μL) was placed in a 24-well cell culture plate, and 1 mL bacterial suspension ($1 \times 10^8$ CFU/mL) was added to a 24-well plate. After incubation at 37 °C for 12 h. After 24 h of incubation at 37 °C, 100 μL of bacterial solution was added to LB agar plates and incubated in a bacterial incubator at 37 °C for 24 h. The colonies on the plate were counted and photographed. Antibacterial viability was calculated using the following formula:

$$\text{Antibacterial viability } (\%) = B_s / B_c \times 100\%$$

$B_s$ and $B_c$ are the colony numbers for the experimental and control groups, respectively.

### 2.7. Biocompatibility test in vitro

The biocompatibility of hydrogels was evaluated using the indirect contact method (sample extracts) and direct contact method. The indirect contact method was as follows: L929 cells were seeded in 24-well culture plates ($5 \times 10^4$ cells) and then treated with different hydrogel extracts (hydrogel: DMEM at a mass ratio of 1:5) for 1, 2 and 3 days. Subsequently, 10 μL CCK-8 solution was added to the cells in each well. After 2 h of incubation, the absorbance was measured at 450 nm using a microplate reader. The cell viability was calculated using the following formula:

$$\text{Cell viability } (\%) = A_s / A_c \times 100\%$$

As and Ac are the absorbance for the experimental and control groups, respectively.

The direct contact method was as follows: the hydrogel was placed in a 24-well plate, and then the L929 cell suspension ($5 \times 10^4$ cells) was added to the surface of the hydrogel. After 1, 2 and 3 days of incubation, the cells were stained with a live-dead cell staining kit and the Actin Cytoskeleton Staining Kit according to the manufacturer's instructions (Biyuntian, Shanghai, China). The medium was changed every two days. Finally, the stained cells were observed under an inverted fluorescence microscope (Nikon TE 2000-U, Tokyo, Japan).

### 2.8. Cell migration study

The migration capability of L929 cells was assessed with a scratch wound assay [31]. L929 cells were seeded in 24-well plates ($1 \times 10^5$ cells/well) and incubated in FBS-free medium for 24 h. Then, a 20 μL pipette tip was used to create scratches on the cell monolayer. The floating cells and debris were removed by washing with PBS. Next, the cells were treated with different hydrogel extracts. After 8 h, 24 h and 32 h of incubation, the cells were rephotographed with a light microscope, and cell migration was calculated using the following formula:

$$\text{Cell migration } (\%) = \frac{(S_0 - S_t)}{S_0} \times 100\%$$

S0 and St are the scratch area at 0 h and the designated time, respectively.

### 2.9. Tube formation assay in vitro

Matrigel was thawed on ice overnight at 4 °C, and 100 μL of diluted Matrigel was placed in each well of a 48-well plate. Next, 300 μL HUVECs ($1 \times 10^4$ cells) were evenly seeded on Matrigel and treated with hydrogel extract. After 4 h of incubation at 37 °C, tube formation was photographed with a microscope. The number of junctions and total tube length were calculated using ImageJ software. Concentrations of PDGF and VEGF were measured using ELISA kits (Meimian, Jiangsu, China).

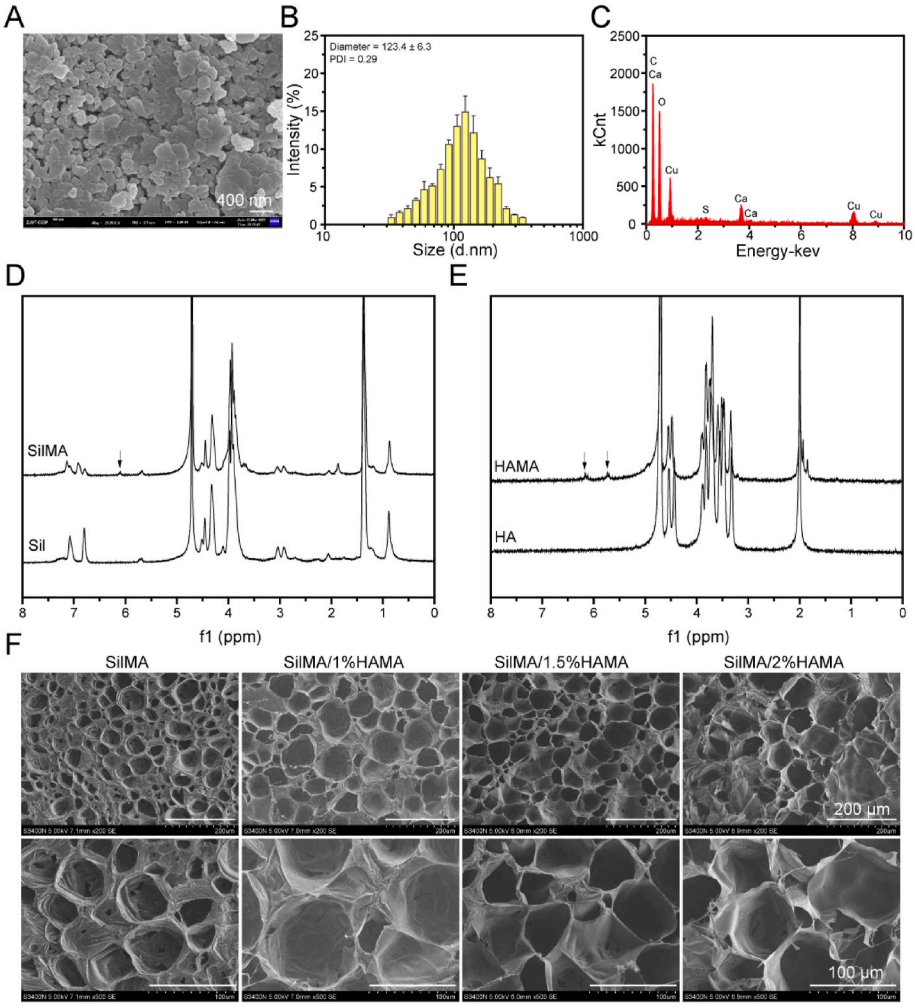


**Fig. 1.** Characterizations of the Cu-EGCG and hydrogels. (A) SEM images of Cu-EGCG. (B) Particle size distribution of Cu-EGCG. (C) EDS image of Cu-EGCG. (D) 1H NMR spectra of Sil and SilMA. (E) 1H NMR spectra of HA and HAMA. (F) SEM image of the hydrogel.

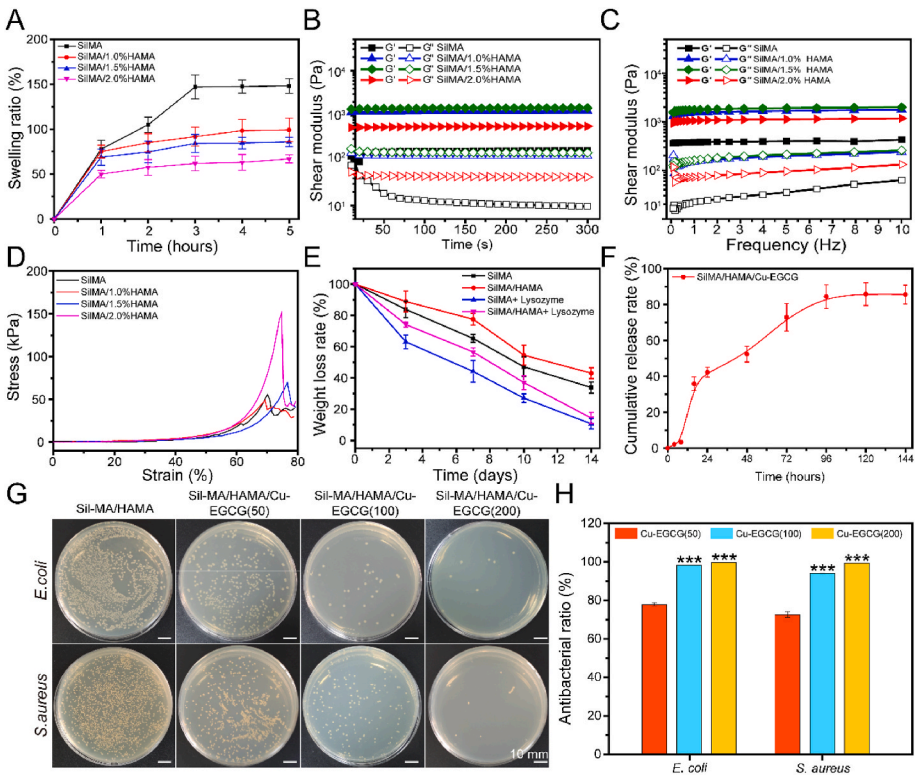


**Fig. 2.** Physical properties, mechanical properties and antimicrobial properties of the hydrogels. (A) The swelling ratio of hydrogels. (B) Rheological properties. (C) Hydrogel viscosity with frequencies ranging from 0.1 to 10 Hz. (D) Compressive curve of hydrogels. (E) The weight loss curve of hydrogels in PBS containing either 0 or 1000 U/mL lysozyme. (F) Cumulative release of $Cu^{2+}$. (G) Images of agar plates of *E. coli* and *S. aureus* treated with SilMA/HAMA/Cu-EGCG hydrogels with different Cu-EGCG concentrations. (H) Antibacterial ratio of *E. coli* and *S. aureus* treated with hydrogels.

### 2.10. Polarization of macrophages

Macrophage RAW 264.7 cells at a density of $5 \times 10^4$ cells were seeded on a 24-well plate and polarized into the M1 type by incubation with 100 ng/mL LPS. Next, the cells were treated with hydrogel extract and incubated for 24 h. The percentage of macrophages with the M1 or M2 subtype was sorted by flow cytometry using antibodies against the M1 macrophage marker (CD86) and the M2 macrophage marker (CD206).

### 2.11. In vivo wound healing assessment

#### 2.11.1. Model establishment

All animal experimental protocols were reviewed and approved by the Animal Protection and Use Committee of Ruige Biotechnology. First, female Sprague–Dawley (SD) rats were anesthetized by intraperitoneal injection (1% sodium pentobarbital, 45 mg/kg). The hair around the surgical site was shaved using an animal electric shaver, followed by hair removal with a Veet depilation cream. Four round model wounds (12 mm) with skin defects were made on both sides of the back of each rat, followed by adding 40 μL of mixed bacteria *E. coli* ($1 \times 10^8$ CFU/mL) and *S. aureus* ($1 \times 10^8$ CFU/mL). After 24 h of infection, the wounds were treated with gauze, Cu-EGCG, SilMA/HAMA, SilMA/HAMA/Cu-EGCG and Aquacel Ag. Finally, the wound was covered with Tegaderm dressing (3 M Company). At specific time points, the wound was observed and photographed with a camera, and the wound area was evaluated using IPP 6.0 software. The rats were euthanized on the 3rd, 7th, 10th and 14th days after hydrogel treatment, and the wounds and surrounding healthy skin tissue were excised for subsequent experiments.

#### 2.11.2. In vivo evaluation of antimicrobial efficacy

To determine bacterial growth in rat wounds, skin tissue from day 3 was homogenized with 2 mL of sterile saline, followed by serial dilutions of the tissue homogenate. One hundred microliters of homogenate were placed on gram-negative bacterial selection medium (selective culture of *E. coli*) and mannitol salt agar medium plates (selective culture of *S. aureus*). The plates were placed in a 37 °C biochemical incubator for upside-down culture. After 24 h of culture, the number of bacteria on the medium was observed and recorded.

#### 2.11.3. Histology analysis

Skin samples were first fixed in 4% paraformaldehyde, dehydrated in graded ethanol and xylene, embedded in paraffin, and cut into 4 μm sections. The sections were stained with hematoxylin and eosin (H&E) and Masson staining for histological study. Finally, the images were collected and analyzed under a microscope.

#### 2.11.4. Immunohistochemistry evaluation

For immunohistochemistry, paraffin sections were deparaffinized, antigen retrieved, fixed with 3% BSA, and then blocked for 30 min at room temperature. Sections were then incubated with primary antibodies (α-SMA, CD31, IFN-γ, TNF-α, IL-4, TGF-β1, CD206, CD68 and iNOS), washed with PBS and then incubated with secondary antibodies. Finally, the nuclei were counterstained with DAPI, and images of the stained samples were collected with an inverted fluorescence microscope (Nikon TE2000-S, Japan) after mounting.

### 2.12. Statistical analysis

All experiments were repeated three times or more. Data are expressed as the mean ± standard deviation (SD), and statistical significance was analyzed using R software (R version 3.5.3). A p value of $<0.05$ was considered statistically significant, and * represents $p < 0.05$, ** represents $p < 0.01$, and *** represents $p < 0.005$.

## 3. Results and discussion

### 3.1. Characterization of the hydrogel

The purpose of promoting wound angiogenesis and inhibiting inflammation is to accelerate wound healing. In this study, EGCG and

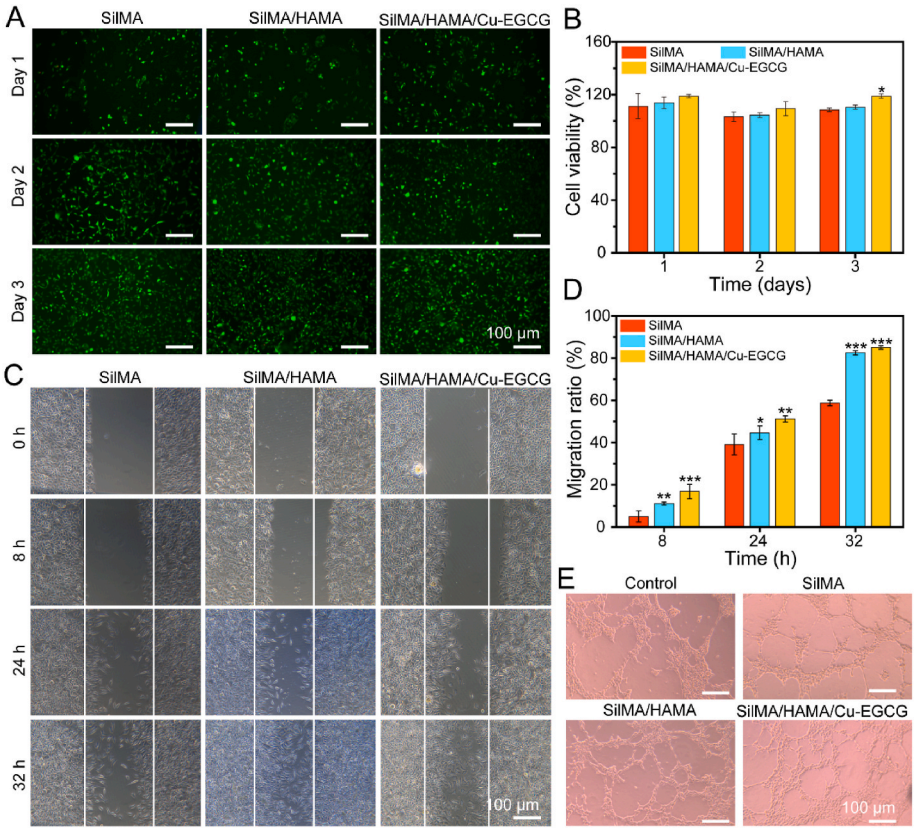


**Fig. 3.** *In vitro* biocompatibility, migration and vascularization evaluation of the hydrogels. (A) Live/dead staining images of L929 cells cultured on hydrogels versus different culture times. (B) Cell viability of L929 cells cultured on hydrogels by CCK-8 assay. (C) Scratch test. (D) Quantitative analysis of the cell migration ratio. (E) Representative image of vascular network formation of HUVECs *in vitro*.

copper ions were utilized to construct coordination networks to form metal polyphenol capsules. Scanning electron microscopy confirmed the microscopic morphology of metal polyphenol-encapsulated Cu-EGCG nanostructures (Fig. 1A). From the dynamic light scattering (DLS) data, the average size of Cu-EGCG was 123.4 ± 5.3 nm, and the PDI was 0.29 (Fig. 1B). EDS confirmed the presence of copper in Cu-EGCG, accounting for 8.2% (Fig. 1C).

To accurately deliver EGCG to the wound site and release polyphenols in a controlled-release manner, SilMA/HAMA hydrogels were developed to load metal polyphenol capsules. The composite crosslinking of SilMA and HAMA can form a double network hydrogel with good biocompatibility and better mechanical properties. In this study, GMA was used to modify silk fibroin to obtain SilMA, and MA was used to modify hyaluronic acid to obtain HAMA. Fig. 1D shows the appearance of a hydrogen absorption peak (6.11 ppm) on the methyl acrylyl group, indicating that the methyl acrylyl group was successfully grafted onto sil, which confirmed the successful preparation of SilMA [32]. Fig. 1E shows the absorption peaks of the methacrylate group (δ = 5.72 ppm and 6.19 ppm), verifying the successful binding of methacrylate-related motifs to HA [32].

In the presence of the LAP photoinitiator and ultraviolet light, the SilMA/HAMA solution formed a stable hydrogel (Fig. S1). The morphological characteristics of SilMA/HAMA hydrogels after lyophilization were observed by SEM. SEM images of hydrogels showed interconnected and uniform porous microstructures (Fig. 1F). The pore size increases with the addition of HAMA (Fig. S2), which is due to the enhanced degree of crosslinking of the SilMA/HAMA hydrogel and the change in the internal structure of the hydrogel. This loose and porous network structure facilitates cell adhesion and migration, maintains a moist environment, absorbs wound exudate, and accelerates wound healing [33,34].

### 3.2. Swelling property test of hydrogels

Hydrogels swell to different degrees in the environment of body fluids. The proper swelling rate is very important to maintain the structure of hydrogels [35]. Fig. 2A shows that the swelling ratio of SilMA/HAMA hydrogels decreases with increasing HAMA concentration. The addition of HAMA resulted in the formation of hydrogels with higher crosslinking strength, so the equilibrium swelling ratio of the hydrogels decreased. All hydrogels reached the swelling equilibrium state at 3 h and maintained a stable swelling rate in the subsequent time, which indicated that the hydrogels had relatively good dimensional stability. Good swelling properties are beneficial for the hydrogel dressing to absorb wound exudate [36].

### 3.3. Rheological and compression analysis

When the elastic modulus is greater than the viscosity modulus, the hydrogels are in the gel state. When the hydrogels are gelatinized, G′ is always greater than G″ with increasing time and angular frequency, indicating that the hydrogels can stably appear in the gel state (Fig. 2B and C). The ideal hydrogel should have good mechanical properties to maintain its convenience and integrity [37]. As shown in Fig. 2D, the compressive strength of the SilMA hydrogel was 70.1 kPa. In addition, the SilMA/1.5%HAMA hydrogel had a maximum compression performance of 151 kPa compared with the other groups, which could be because the SilMA/1.5%HAMA hydrogel may have a good crosslinking degree and the best mechanical properties. All results showed that the compressive strength of the SilMA/HAMA hydrogel can be adjusted by changing the concentration of HAMA, and the adjustable compressive strength of the material means that it can be better applied to various tissues and organs, making it a biomaterial with a number of current and

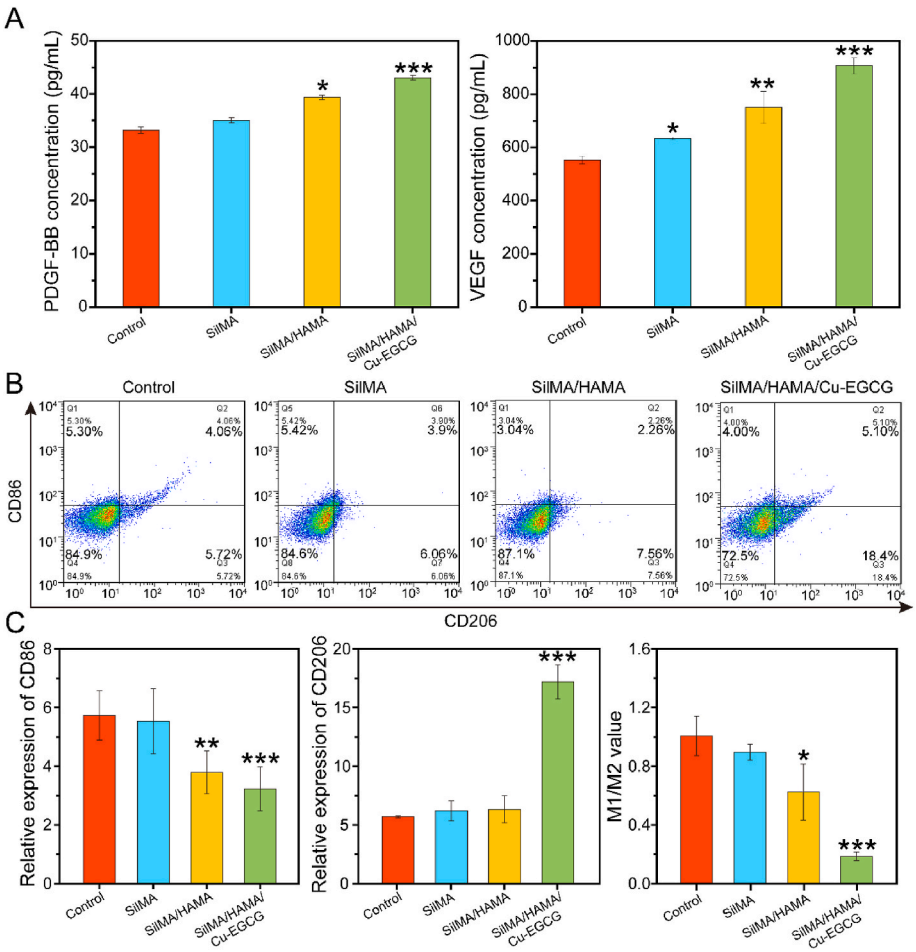


**Fig. 4.** The evaluation of macrophage polarization in RAW264.7 cell. (A) PDGF-BB and VEGF concentrations by ELISA. (B) CD86 and CD206 expression on RAW 264.7 cells were analyzed by flow cytometry. (C) Relative expression of CD86, CD206 and M1/M2 value according to flow cytometry results.

potential biomedical applications [38].

### 3.4. Degradation and release of $Cu^{2+}$ from hydrogels in vitro

The degradation curves of SilMA and SilMA/1.5%HAMA hydrogels in the absence of lysozyme and the concentration of lysozyme at 1000 U/mL are shown in Fig. 2E. In addition, the weight loss rate of the hydrogels with lysozyme was faster than that without the enzyme. The degradation rate of the SilMA/1.5%HAMA hydrogel group was relatively slower than that of the pure SilMA hydrogel group, which should be attributed to the relatively higher degree of cross-linking of these two groups of hydrogels. Fig. 2F shows the release curve of Cu-EGCG loaded with the hydrogel. The release of $Cu^{2+}$ tends to be flat after 96 h, indicating that the release of $Cu^{2+}$ is effectively prolonged under the dual action of hydrogel and metal polyphenol capsules [25].

### 3.5. Antibacterial activity evaluation

Microbial infection is the main challenge of wound healing [5]. The ideal wound dressing should have good antibacterial properties to promote wound healing [39]. As shown in Fig. 2G and H, the colony map of *E. coli* was similar to that of *S. aureus*. Compared with the SilMA/HAMA control group, the SilMA/HAMA/Cu-EGCG hydrogel had a better antibacterial effect, among which the SilMA/HAMA/Cu-EGCG (200) hydrogel had the best antibacterial effect, and the colonies of *E. coli* and *S. aureus* on agar plates were the least abundant. We speculated that the reason for the high antibacterial activity of the SilMA/HAMA/Cu-EGCG hydrogel is that the Cu-EGCG in the hydrogel can release $Cu^{2+}$ into the bacteria and interact with the proteins in the bacteria and the phosphorus and sulfur groups of DNA, thus producing excellent antibacterial activity [40,41].

### 3.6. Biocompatibility evaluation

Biocompatibility is an important factor for the safe application of hydrogels in biomedicine [42]. As shown in Fig. S3, the concentration of 100 μg/mL Cu-EGCG was selected as the optimal concentration for the following experiment. As shown in Fig. 3A, after coculture of hydrogel and L929 cells for 3 days, the cell survival rate reached more than 100%, indicating that the hydrogel had no toxicity and was conducive to cell proliferation. After culture with L929 cells for 3 days, almost all hydrogels expressed green fluorescence, and few cells died (Fig. 3B). The actin cytoskeleton staining images showed that the cells were attached to the hydrogel and were able to spread at 1, 2 and 3 days (Fig. S4). All experimental results showed that the SilMA/HAMA/Cu-EGCG hydrogel had good biocompatibility and promoted cell proliferation to provide a favorable environment for cell growth, so it has the potential to be used as a hydrogel dressing.

### 3.7. Cell migration, scratch and macrophage polarization assay

The effect of the hydrogel on L929 migration was evaluated by a scratch test. The number of migrating cells in the SilMA/HAMA/Cu-EGCG group was significantly higher than that in the SilMA group, and the ability of the samples in each group to promote the migration of L929 cells was in the order of SilMA/HAMA/Cu-EGCG > SilMA/HAMA

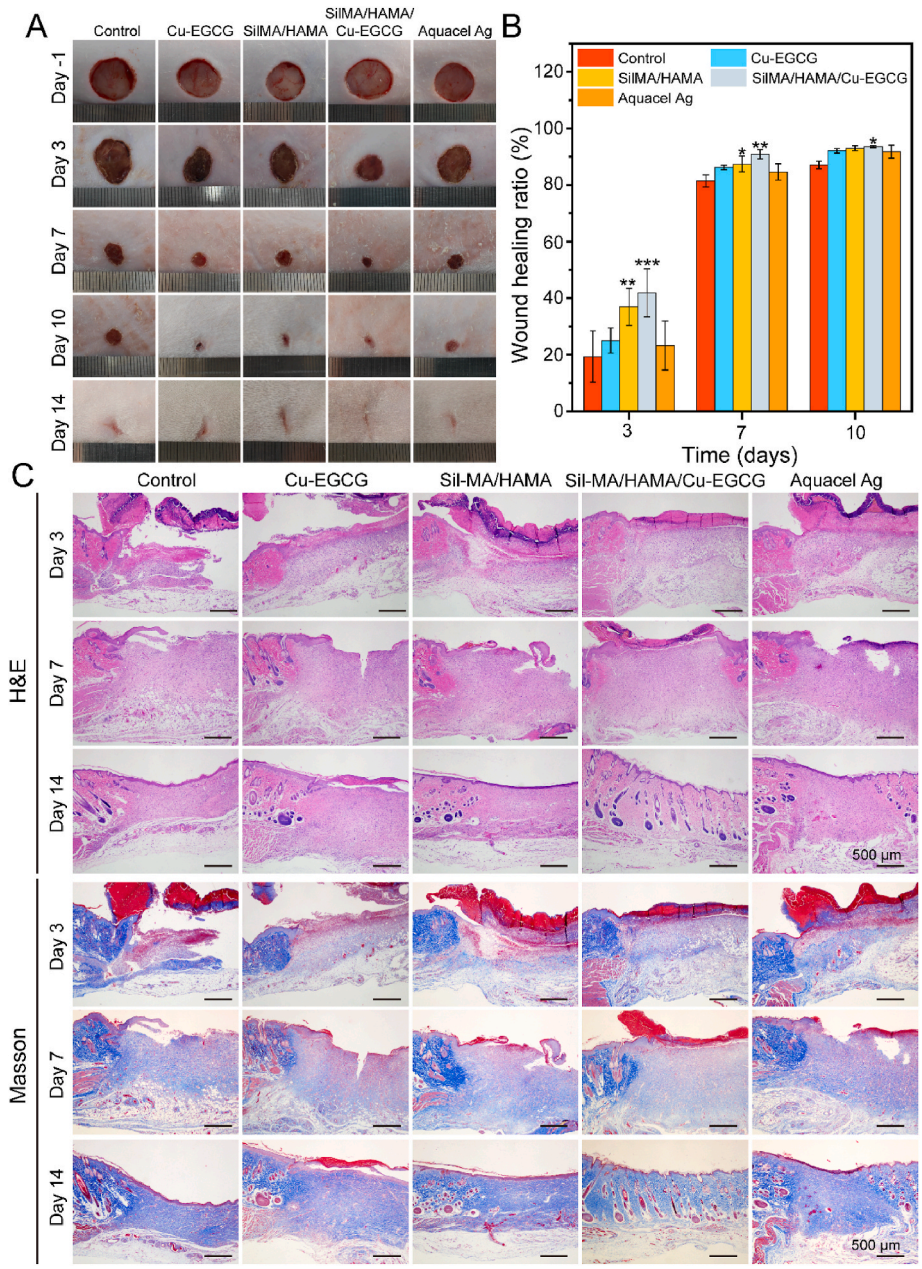


**Fig. 5.** *In vivo* infected wound healing studies of the hydrogels. (A) Photographs of wounds treated with the different materials on days −1, 3, 7, 10 and 14. (B) Wound healing ratio under the treatment of different dressings on different days. (C) HE staining and Masson staining on days 3, 7, and 14 of the newly regenerated skin tissues for each group.

> SilMA (Fig. 3C). The mobility of SilMA/HAMA/Cu-EGCG reached 80% or more within 32 h (Fig. 3D), which indicates that hydrogel samples can promote cell proliferation.

In addition, the angiogenic properties of the prepared materials were evaluated by tube-forming experiments using matrix glue. As shown in Fig. 3E, compared with the SilMA group, the effect of the SilMA/HAMA groups on tubule formation was very small, while the SilMA/HAMA/Cu-EGCG group had obvious tubule formation and branching points (Fig. S5), which may be because of Cu-EGCG on blood vessel formation. As compared to the blank control group cultured with HUVECs without hydrogel extract, SilMA/HAMA/Cu-EGCG group showed the highest concentration of PDGF-BB and VEGF (Fig. 4A), which was due to that $Cu^{2+}$ could increase the expression level of PDGF-BB and VEGF [25].

According to different functions and phenotypes, Macrophages can be divided into proinflammatory classically activated (M1, CD68) and anti-inflammatory alternatively activated (M2, CD206) macrophages [43,44]. Fig. 4B and C showed macrophages treated with the SilMA/HAMA/Cu-EGCG hydrogel could upregulate of CD206 expression levels and downregulate of CD86 levels. These results suggest that the SilMA/HAMA/Cu-EGCG hydrogel has the intrinsic ability to reculture macrophages from the M2 phenotype to the M1 phenotype.

### 3.8. Wound healing examination

On the -1st day, the initial wound size of the five groups was basically the same (Fig. 5A). On the 3rd day, there was no obvious contraction in the blank control group, wound healing was better in the SilMA/HAMA/Cu-EGCG hydrogel group (41.7%) and SilMA/HAMA group (38.6%), which were significantly higher than those of the blank control group (19.3%) (Fig. 5B). On the 7th day, all the wounds in the five groups began to form scabs, and the wounds contracted obviously, among which the hydrogel group healed the best. On the 14th day, the hydrogel

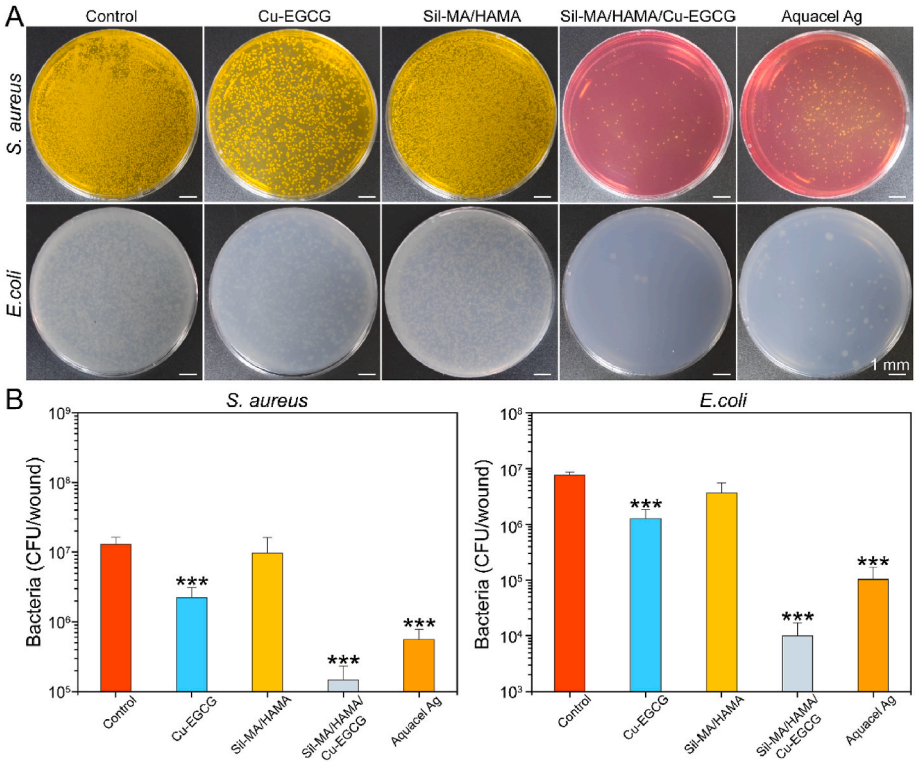


**Fig. 6.** Bacterial quantification of wound tissues. (A) Digital images of colony forming units of *E. coli* and *S. aureus* were obtained from wound tissue at day 3. (B) Quantitative results of agar plate counting after 24 h.

group showed the smallest scar area. Prior studies have shown that the release of $Cu^{2+}$ in the hydrogel to the wound site could promote wound healing [45]. In addition, electroactive materials could also accelerate wound healing. The above results showed that the synergistic effect of $Cu^{2+}$ and EGCG in hydrogels can promote the healing of infected wounds.

### 3.9. Histological analysis

To further study the effect of the hydrogel on wound healing, the

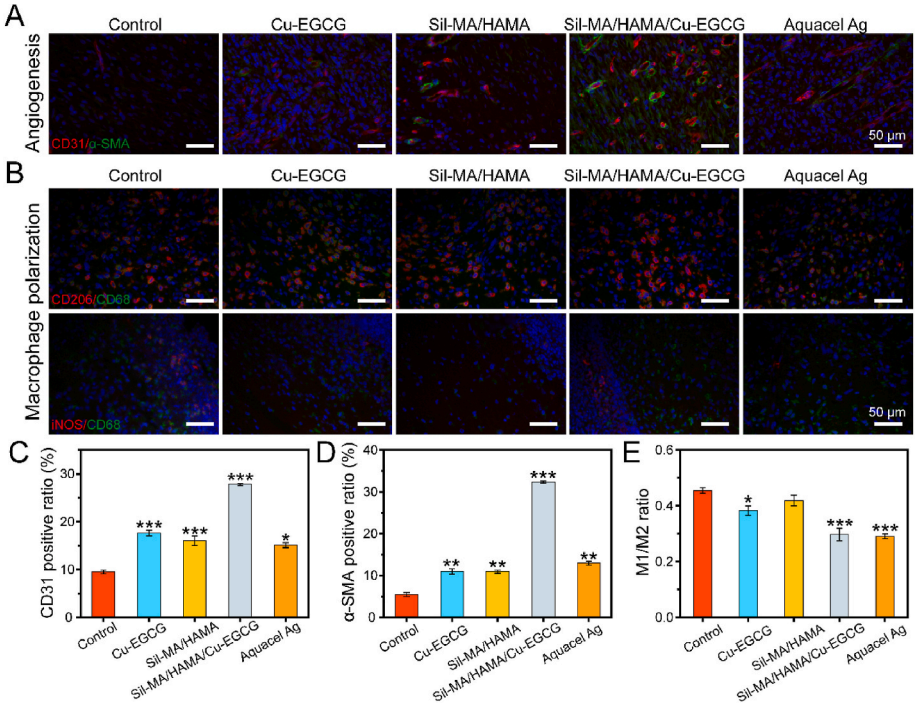


**Fig. 7.** Immunofluorescence staining study of wound healing. (A) Immunofluorescence staining of CD31 and α-SMA in wounds on day 7. (B) Immunofluorescence staining of CD206/CD68 and iNOS/CD68 in wounds on day 3. (C) Quantitative analysis of CD31. (D) Quantitative analysis of α-SMA. (E) Quantitative analysis of M1/M2.

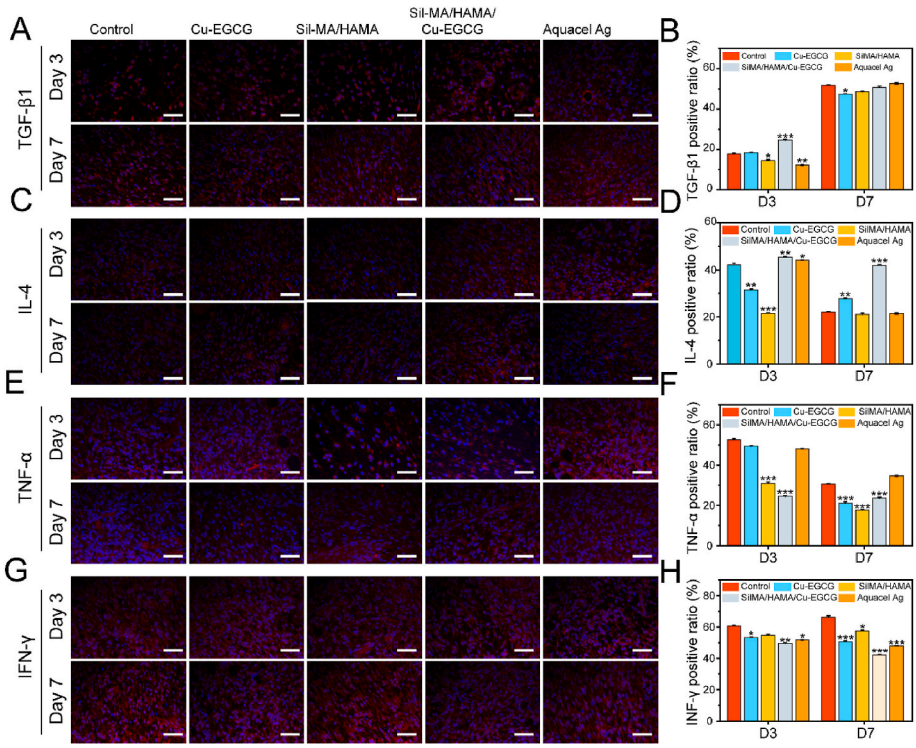


**Fig. 8.** Immunofluorescence staining study of inflammatory levels. Immunofluorescence staining of TGF-β1 (A), IL-4 (C), TNF-α (E) and IFN-γ (G) in wounds on day 3 and day 7. Quantitative analysis of TGF-β1 (B), IL-4 (D), TNF-α (F) and IFN-γ (H) in wounds on day 3 and day 7 by immunofluorescence staining.

wound healing process was observed by hematoxylin eosin (H&E) and Masson staining. The thickness of granulation tissue on the 3rd day compared with the control group indicated different degrees of wound healing in each group (Fig. 5C), which indicated that all rats had normal metabolic function. The thickness of granulation tissue in the SilMA/HAMA/Cu-EGCG group was larger than that in the different groups on the 7th day, and the growth of capillaries and the recovery of skin appendages were observed on the 14th day, which indicated that the wound tissue slices in the SilMA/HAMA/Cu-EGCG group showed a faster healing effect.

In addition, Masson staining was performed on different groups to reflect the deposition of collagen. As one of the main components of the dermis, collagen deposition plays an important role in wound healing. The increase in collagen content in the wound further promoted faster wound regeneration. Additionally, in the SilMA/HAMA/Cu-EGCG group, the area of collagen deposition at the wound was larger, and the collagen fibers were dense.

### 3.10. Analysis of antibacterial properties in vivo

In addition to being able to resist external bacteria from entering the wound tissue, wound dressings should also have effective antibacterial properties. As shown in Fig. 6A and B, the number of colonies of *E. coli* and *S. aureus* of SilMA/HAMA/Cu-EGCG was much smaller than that of the other groups, and the statistics further showed that the bacterial survival rate of the SilMA/HAMA/Cu-EGCG group was extremely low, which demonstrated that SilMA/HAMA/Cu-EGCG has excellent antibacterial properties. Prior studies showed the antimicrobial principle of Cu-EGCG as follows: First, the direct interaction between the copper surface and the bacterial outer membrane caused the rupture of the bacterial outer membrane. Then, the copper surface acts on the holes in the bacteria's outer membrane, depriving the cells of essential nutrients and water, resulting in shrinking [46].

### 3.11. Immunofluorometric assay

In the proliferative phase, the formation of new capillaries, the remodeling of blood vessels, and the formation of new granulation tissue are necessary processes for wound healing. The formation of new blood vessels is a key factor in wound healing [47,48]. As shown in Fig. 7A, more new blood vessels were observed in the SilMA/HAMA/Cu-EGCG group-covered wounds than in the other groups. Quantitative analysis of immunofluorescence staining showed that the expression levels of CD31 and α-SMA in the SilMA/HAMA/Cu-EGCG group were significantly higher than those in the other groups on day 7 (Fig. 7C and D). The results showed that the SilMA/HAMA/Cu-EGCG hydrogel has a good ability to promote angiogenesis and is more conducive to promoting the three-dimensional assembly and reconstruction of the vascular network, which can provide nutrients for the regeneration of epithelial cells, accelerate the process of re-epithelialization, and significantly promote wound healing [49,50].

Macrophages have two different phenotypes, namely, proinflammatory (M1) and anti-inflammatory (M2) phenotypes, and the transformation of macrophages from the M1 phenotype to the M2 phenotype is a potential method to treat inflammation [46,51]. As shown in Fig. 7B and E, the iNOS (M1 marker) signal in the SilMA/HAMA/Cu-EGCG group decreased, and the CD68 (M2 marker) signal became apparent compared to other groups, indicating that the macrophages were effectively repolarized from M1 to M2. The results indicated that the SilMA/HAMA/Cu-EGCG group could play an anti-inflammatory role by regulating the polarization of macrophages and then regulating the expression of inflammatory cytokines. Therefore, changing the immunoregulatory balance between M1 and M2 macrophages, resulting in faster and larger M2 macrophage infiltration, which may be a potentially beneficial trigger for rapid angiogenesis and treatment of diabetic wound healing.

The inflammatory level of rat wounds was further evaluated by immunofluorescence staining. TGF-β1 triggers fibroblasts and myofibroblasts to produce new ECM, which plays a central role in

fibrinogenesis [52]. In addition, IL-4 is an anti-inflammatory cytokine that can induce polarization of macrophages [53]. The expression of TGF-β1 and IL-4 at the wound site in the SilMA/HAMA/Cu-EGCG group was significantly upregulated and was highest (Fig. 8A–D). TNF-α and IFN-γ are markers of inflammation, which involved in regulating the immune response, cell survival and apoptosis [54]. Meanwhile, the expression of TNF-α and IFN-γ at the wound site in the SilMA/HAMA/Cu-EGCG group was significantly downregulated and was the lowest (Fig. 8E–H). In summary, SilMA/HAMA/Cu-EGCG can regulate the secretion of anti-inflammatory cytokines, inhibit the expression of TNF-α, change the wound microenvironment from a proinflammatory state to a promlytic state, and promote matrix regeneration and vascular remodeling.

## 4. Conclusions

The purpose of this study was to construct a controlled-release antibacterial compound hydrogel for promoting chronic wound healing. The SilMA/HAMA hydrogel was successfully prepared by a light curing method and loaded with metal polyphenol capsules (Cu-EGCG) to achieve sustained release of copper ions. The hydrogel has good mechanical properties and biocompatibility. Hydrogel containing Cu-EGCG can significantly promote the proliferation and migration of L929 fibroblasts. The antibacterial activity *in vitro* and *in vivo* showed that the hydrogel containing Cu-EGCG had excellent antibacterial activity and effectively reduced the number of bacteria in infected wounds of rats. The results of animal experiments showed that the SilMA/HAMA/Cu-EGCG hydrogel can promote infected wound healing in rats, increase collagen deposition, promote angiogenesis, reduce bacterial numbers, and balance inflammatory infiltration. All results showed that the SilMA/HAMA/Cu-EGCG hydrogel with good biological activity and antibacterial properties has great potential in accelerating wound healing, especially in infected wounds.

## CRediT authorship contribution statement

**Nanbo Liu:** Conceptualization, Methodology, Software, Data curation, Writing – original draft. **Shuoji Zhu:** Conceptualization, Methodology, Software, Data curation, Writing – original draft. **Yuzhi Deng:** Conceptualization, Methodology, Software, Data curation, Writing – original draft. **Ming Xie:** Conceptualization, Methodology, Software, Data curation, Writing – original draft. **Mingyi Zhao:** Visualization, Investigation, Supervision. **Tucheng Sun:** Software, Validation. **Changjiang Yu:** Software, Validation. **Ying Zhong:** Software, Validation. **Rui Guo:** Writing – review & editing. **Keluo Cheng:** Writing – review & editing. **Dehua Chang:** Writing – review & editing. **Ping Zhu:** Writing – review & editing.

## Declaration of competing interest

The authors declare no competing financial interest.

## Acknowledgments

This research was funded by National Key Research and Development Program of China (2017YFA0105602, 2018YFA0108700), NSFC Projects of INTERNATIONAL COOPERATION and Exchanges (81720108004), National Natural Science Foundation of China (81974019,82100275), Guangdong Provincial Special Support Program for Prominent Talents (2021JC06Y656), Science and Technology Planning Project of Guangdong Province (2020B1111170011, 2022B1212010010), Guangdong special funds for science and technology innovation strategy, China (Stability support for scientific research institutions affiliated to Guangdong Province-GDCI 2021), Guangzhou Science and Technology Plan Project (202201000006), The Special Project of Dengfeng Program of Guangdong Provincial People's Hospital (DFJH201812,KJ012019119, KJ012019423). The Marine Economy Development Project of Department of Natural Resources of Guangdong Province (No. GDNRC [2022]039).

## Appendix A. Supplementary data

Supplementary data to this article can be found online at https://doi.org/10.1016/j.bioactmat.2022.12.009.

## References

[1] S. Chen, L. Sun, X. Zhou, Y. Guo, J. Song, S. Qian, Z. Liu, Q. Guan, E. Meade Jeffries, W. Liu, Y. Wang, C. He, Z. You, Mechanically and biologically skin-like elastomers for bio-integrated electronics, Nat. Commun. 11 (1) (2020) 1107.
[2] Y. Gu, J. Han, C. Jiang, Y. Zhang, Biomarkers, oxidative stress and autophagy in skin aging, Ageing Res. Rev. 59 (2020), 101036.
[3] F. Qu, R. Geng, Y. Liu, J. Zhu, Advanced nanocarrier- and microneedle-based transdermal drug delivery strategies for skin diseases treatment, Theranostics 12 (7) (2022) 3372–3406.
[4] Y. Luo, J. Li, X. Liu, L. Tan, Z. Cui, X. Feng, X. Yang, Y. Liang, Z. Li, S. Zhu, Y. Zheng, K.W.K. Yeung, C. Yang, X. Wang, S. Wu, Dual metal-organic framework heterointerface, ACS Cent. Sci. 5 (9) (2019) 1591–1601.
[5] M. Bagheri, M. Validi, A. Gholipour, P. Makvandi, E. Sharifi, Chitosan nanofiber biocomposites for potential wound healing applications: antioxidant activity with synergic antibacterial effect, Bioeng. Transl. Med. 7 (1) (2022), e10254.
[6] A.M. Cheverton, B. Gollan, M. Przydacz, C.T. Wong, A. Mylona, S.A. Hare, S. Helaine, A Salmonella toxin promotes persister formation through acetylation of tRNA, Mol. Cell 63 (1) (2016) 86–96.
[7] A.A. Ordonez, M.A. Sellmyer, G. Gowrishankar, C.A. Ruiz-Bedoya, E.W. Tucker, C. J. Palestro, D.A. Hammoud, S.K. Jain, Molecular imaging of bacterial infections: overcoming the barriers to clinical translation, Sci. Transl. Med. 11 (508) (2019).
[8] Y. Qiao, X. Liu, B. Li, Y. Han, Y. Zheng, K.W.K. Yeung, C. Li, Z. Cui, Y. Liang, Z. Li, S. Zhu, X. Wang, S. Wu, Treatment of MRSA-infected osteomyelitis using bacterial capturing, magnetically targeted composites with microwave-assisted bacterial killing, Nat. Commun. 11 (1) (2020) 4446.
[9] N. Wali, A. Shabbir, N. Wajid, N. Abbas, S.Z.H. Naqvi, Synergistic efficacy of colistin and silver nanoparticles impregnated human amniotic membrane in a burn wound infected rat model, Sci. Rep. 12 (1) (2022), 6414-6414.
[10] S.Y. Chae, R. Park, S.W. Hong, Surface-mediated high antioxidant and anti-inflammatory effects of astaxanthin-loaded ultrathin graphene oxide film that inhibits the overproduction of intracellular reactive oxygen species, Biomater. Res. 26 (1) (2022) 30.
[11] S.Y. Wang, H. Kim, G. Kwak, H.Y. Yoon, S.D. Jo, J.E. Lee, D. Cho, I.C. Kwon, S. H. Kim, Development of biocompatible HA hydrogels embedded with a new synthetic peptide promoting cellular migration for advanced wound care management, Adv. Sci. 5 (11) (2018), 1800852.
[12] C. Zhu, S. Zou, Z. Rao, L. Min, M. Liu, L. Liu, L. Fan, Preparation and characterization of hydroxypropyl chitosan modified with nisin, Int. J. Biol. Macromol. 105 (Pt 1) (2017) 1017–1024.
[13] C. Dai, Y. Wang, Y. Shan, C. Ye, Z. Lv, S. Yang, L. Cao, J. Ren, H. Yu, S. Liu, Z. Shao, J. Li, W. Chen, S. Ling, Cytoskeleton-inspired hydrogel ionotronics for tactile perception and electroluminescent display in complex mechanical environments, Mater. Horiz. (2022) 2051–6347.
[14] C. Fan, Q. Xu, R. Hao, C. Wang, Y. Que, Y. Chen, C. Yang, J. Chang, Multi-functional wound dressings based on silicate bioactive materials, Biomaterials 287 (2022), 121652.
[15] Q. Wen, S. Mithieux, A. Weiss, Elastin biomaterials in dermal repair, Trends Biotechnol. 38 (3) (2020) 280–291.
[16] H. Wang, Y. Wu, C. Cui, J. Yang, W. Liu, Antifouling super water absorbent supramolecular polymer hydrogel as an artificial vitreous body, Adv. Sci. 5 (11) (2018), 1800711.
[17] D. Hanjaya-Putra, V. Bose, Y.I. Shen, J. Yee, S. Khetan, K. Fox-Talbot, C. Steenbergen, J.A. Burdick, S. Gerecht, Controlled activation of morphogenesis to generate a functional human microvasculature in a synthetic matrix, Blood 118 (3) (2011) 804–815.
[18] M.E. Ramos-Nino, S.R. Blumen, H. Pass, B.T. Mossman, Fra-1 governs cell migration via modulation of CD44 expression in human mesotheliomas, Mol. Cancer 6 (2007) 81.
[19] P. Jamalzaei, M. Rezazadeh Valojerdi, L. Montazeri, H. Baharvand, Applicability of hyaluronic acid-alginate hydrogel and ovarian cells for in vitro development of mouse preantral follicles, Cell J 22 (Suppl 1) (2020) 49–60.
[20] S. Vijayavenkataraman, Nerve guide conduits for peripheral nerve injury repair: a review on design, materials and fabrication methods, Acta Biomater. 106 (2020) 54–69.
[21] Q. Lin, J.Y.C. Lim, K. Xue, X. Su, X.J. Loh, Polymeric hydrogels as a vitreous replacement strategy in the eye, Biomaterials 268 (2021), 120547.
[22] S.H. Choi, S.W. Kim, Z. Ku, M.A. Visbal-Onufrak, S.R. Kim, K.H. Choi, H. Ko, W. Choi, A.M. Urbas, T.W. Goo, Y.L. Kim, Anderson light localization in biological nanostructures of native silk, Nat. Commun. 9 (1) (2018) 452.
[23] H. Wang, D. Wang, B. Luo, D. Wang, H. Jia, P. Peng, Q. Shang, J. Mao, C. Gao, Y. Peng, L. Gan, J. Du, Z. Luo, L. Yang, Decoding the annulus fibrosus cell atlas by scRNA-seq to develop an inducible composite hydrogel: a novel strategy for disc reconstruction, Bioact. Mater. 14 (2022) 350–363.

[24] B.M. Weiss, S.W. Wong, R.L. Comenzo, Beyond the plasma cell: emerging therapies for immunoglobulin light chain amyloidosis, Blood 127 (19) (2016) 2275–2280.
[25] J. Duan, Z. Chen, X. Liang, Y. Chen, H. Li, X. Tian, M. Zhang, X. Wang, H. Sun, D. Kong, Y. Li, J. Yang, Construction and application of therapeutic metal-polyphenol capsule for peripheral artery disease, Biomaterials 255 (2020), 120199.
[26] R. Xu, K. Yang, S. Li, M. Dai, G. Chen, Effect of green tea consumption on blood lipids: a systematic review and meta-analysis of randomized controlled trials, Nutr. J. 19 (1) (2020) 48.
[27] C. Opuwari, T. Monsees, Green tea consumption increases sperm concentration and viability in male rats and is safe for reproductive, liver and kidney health, Sci. Rep. 10 (1) (2020), 15269.
[28] Y. Ju, C. Cortez-Jugo, J. Chen, T.Y. Wang, A.J. Mitchell, E. Tsantikos, N. Bertleff-Zieschang, Y.W. Lin, J. Song, Y. Cheng, S. Mettu, M.A. Rahim, S. Pan, G. Yun, M. L. Hibbs, L.Y. Yeo, C.E. Hagemeyer, F. Caruso, Engineering of nebulized metal-phenolic capsules for controlled pulmonary deposition, Adv. Sci. 7 (6) (2020), 1902650.
[29] N. Qin, S. Zhang, J. Jiang, S.G. Corder, Z. Qian, Z. Zhou, W. Lee, K. Liu, X. Wang, X. Li, Z. Shi, Y. Mao, H.A. Bechtel, M.C. Martin, X. Xia, B. Marelli, D.L. Kaplan, F. G. Omenetto, M. Liu, T.H. Tao, Nanoscale probing of electron-regulated structural transitions in silk proteins by near-field IR imaging and nano-spectroscopy, Nat. Commun. 7 (2016), 13079.
[30] C. Li, C. Li, Z. Ma, H. Chen, H. Ruan, L. Deng, J. Wang, W. Cui, Regulated macrophage immune microenvironment in 3D printed scaffolds for bone tumor postoperative treatment, Bioact. Mater. 19 (2022) 474–485, forthcoming.
[31] B. Yang, M. Li, W. Tang, W. Liu, S. Zhang, L. Chen, J. Xia, Dynamic network biomarker indicates pulmonary metastasis at the tipping point of hepatocellular carcinoma, Nat. Commun. 9 (1) (2018) 678.
[32] K. Lu, K. Li, M. Zhang, Z. Fang, P. Wu, L. Feng, K. Deng, C. Yu, Y. Deng, Y. Xiao, P. Zhu, R. Guo, Adipose-derived stem cells (ADSCs) and platelet-rich plasma (PRP) loaded gelatin/silk fibroin hydrogels for improving healing in a murine pressure ulcer model, Chem. Eng. J. 424 (2021), 130429.
[33] Q. Huang, Y. Zou, M.C. Arno, S. Chen, T. Wang, J. Gao, A.P. Dove, J. Du, Hydrogel scaffolds for differentiation of adipose-derived stem cells, Chem. Soc. Rev. 46 (20) (2017) 6255–6275.
[34] S. Jiang, C. Lyu, P. Zhao, W. Li, W. Kong, C. Huang, G.M. Genin, Y. Du, Cryoprotectant enables structural control of porous scaffolds for exploration of cellular mechano-responsiveness in 3D, Nat. Commun. 10 (1) (2019) 3491.
[35] J.A. Beamish, L.C. Geyer, N.A. Haq-Siddiqi, K. Kottke-Marchant, R.E. Marchant, The effects of heparin releasing hydrogels on vascular smooth muscle cell phenotype, Biomaterials 30 (31) (2009) 6286–6294.
[36] L. Zhou, H. Zheng, S. Wang, F. Zhou, B. Lei, Q. Zhang, Biodegradable conductive multifunctional branched poly(glycerol-amino acid)-based scaffolds for tumor/infection-impaired skin multimodal therapy, Biomaterials 262 (2020), 120300.
[37] H. Zhao, H. Feng, J. Liu, F. Tang, Y. Du, N. Ji, L. Xie, X. Zhao, Z. Wang, Q. Chen, Dual-functional guanosine-based hydrogel integrating localized delivery and anticancer activities for cancer therapy, Biomaterials 230 (2020), 119598.
[38] W. Chen, H. Chen, D. Zheng, H. Zhang, L. Deng, W. Cui, Y. Zhang, H.A. Santos, H. Shen, Gene-hydrogel microenvironment regulates extracellular matrix metabolism balance in nucleus pulposus, Adv. Sci. 7 (1) (2020), 1902099.
[39] B. Tao, C. Lin, X. Qin, Y. Yu, A. Guo, K. Li, H. Tian, W. Yi, D. Lei, Y. Chen, L. Chen, Fabrication of gelatin-based and Zn(2+)-incorporated composite hydrogel for accelerated infected wound healing, Mater. Today Bio. 13 (2022), 100216.
[40] R. Yang, G. Li, C. Zhuang, P. Yu, T. Ye, Y. Zhang, P. Shang, J. Huang, M. Cai, L. Wang, W. Cui, L. Deng, Gradient bimetallic ion-based hydrogels for tissue microstructure reconstruction of tendon-to-bone insertion, Sci. Adv. 7 (26) (2021).
[41] X. Lin, H. Zhang, S. Li, L. Huang, R. Zhang, L. Zhang, A. Yu, B. Duan, Polyphenol-driving assembly for constructing chitin-polyphenol-metal hydrogel as wound dressing, Carbohydr. Polym. 290 (2022), 119444.
[42] W. Zhou, Z. Duan, J. Zhao, R. Fu, C. Zhu, D. Fan, Glucose and MMP-9 dual-responsive hydrogel with temperature sensitive self-adaptive shape and controlled drug release accelerates diabetic wound healing, Bioact. Mater. 17 (2022) 1–17.
[43] H. Kim, S. Wang, G. Kwak, Y. Yang, I. Kwon, S.J.A.s. Kim, Exosome-guided phenotypic switch of M1 to M2 macrophages for cutaneous, Wound Healing 6 (20) (2019), 1900513.
[44] W. Liu, R. Gao, C. Yang, Z. Feng, W. Ou-Yang, X. Pan, P. Huang, C. Zhang, D. Kong, W.J.S.a. Wang, Staphylococcus aureusECM-mimetic immunomodulatory hydrogel for methicillin-resistant -infected chronic skin wound healing, 8, 2022, eabn7006, 27.
[45] J. Qian, L. Ji, W. Xu, G. Hou, J. Wang, Y. Wang, T. Wang, Copper-hydrazide coordinated multifunctional hyaluronan hydrogels for infected wound healing, ACS Appl. Mater. Interfaces 14 (14) (2022) 16018–16031.
[46] J. Xie, X. Wu, S. Zheng, K. Lin, J.J.J.o.n. Su, Aligned electrospun poly(L-lactide) nanofibers facilitate wound healing by inhibiting macrophage M1 polarization via the JAK-STAT and NF-κB pathways, J. Nanobiotechnol. 20 (1) (2022) 342.
[47] J. Rebling, M. Ben-Yehuda Greenwald, M. Wietecha, S. Werner, D. Razansky, Long-term imaging of wound angiogenesis with large scale optoacoustic microscopy, Adv. Sci. 8 (13) (2021), 2004226.
[48] A.P. Veith, K. Henderson, A. Spencer, A.D. Sligar, A.B. Baker, Therapeutic strategies for enhancing angiogenesis in wound healing, Adv. Drug Deliv. Rev. 146 (2019) 97–125.
[49] R. Augustine, P. Prasad, I.J.M.s. Khalaf, M.f.b.a. engineering C, Therapeutic angiogenesis: from conventional approaches to recent nanotechnology-based interventions, Mater. Sci. Eng. C 97 (2019) 994–1008.
[50] J.D. Douglass, M.D. Dorfman, R. Fasnacht, L.D. Shaffer, J.P. Thaler, Astrocyte IKKβ/NF-κB signaling is required for diet-induced obesity and hypothalamic inflammation, Mol. Metabol. 6 (4) (2017) 366–373.
[51] Y. Yang, L. Guo, Z. Wang, P. Liu, X. Liu, J. Ding, W. Zhou, Targeted silver nanoparticles for rheumatoid arthritis therapy via macrophage apoptosis and Re-polarization, Biomaterials 264 (2021), 120390.
[52] T. Kamo, H. Akazawa, I. Komuro, Cardiac nonmyocytes in the hub of cardiac hypertrophy, Circ. Res. 117 (1) (2015) 89–98.
[53] Z. Chen, D. Andreev, K. Oeser, B. Krljanac, A. Hueber, A. Kleyer, D. Voehringer, G. Schett, A. Bozec, Th2 and eosinophil responses suppress inflammatory arthritis, Nat. Commun. 7 (2016), 11596.
[54] B. Mathew, S. Ravindran, X. Liu, L. Torres, M. Chennakesavalu, C.C. Huang, L. Feng, R. Zelka, J. Lopez, M. Sharma, S. Roth, Mesenchymal stem cell-derived extracellular vesicles and retinal ischemia-reperfusion, Biomaterials 197 (2019) 146–160.